J MATER RES TECHNOL. 2020;9(6):12783–12794

Available online at www.sciencedirect.com

jmr&t Journal of Materials Research and Technology

https://www.journals.elsevier.com/journal-of-materials-research-and-technology

Original Article

Alkali activated slag cement doped with Zn-rich electric arc furnace dust

Irena Nikolić[a,b,*], *Dijana Đurović*[b], *Smilja Marković*[c], *Liljana Veselinović*[c], *Ivona Janković-Častvan*[d], *Vuk V. Radmilović*[d], *Velimir R. Radmilović*[e]

[a] *University of Montenegro, Faculty of Metallurgy and Technology, Džordža Vašingtona bb, 81000 Podgorica, Montenegro*
[b] *Institut of Public Health of Montenegro, Džona Džeksona bb, 81000 Podgorica, Montenegro*
[c] *Institute of Technical Sciences of Serbian Academy of Sciences and Arts, Knez Mihailova 35/IV, 11000, Belgrade, Serbia*
[d] *Faculty of Technology and Metallurgy, University of Belgrade, Karnegijeva 4, 11120 Belgrade, Serbia*
[e] *Serbian Academy of Sciences and Arts, Knez Mihailova 35, 11000, Belgrade, Serbia*

ARTICLE INFO

Article history:
Received 12 May 2020
Accepted 5 September 2020
Available online 21 September 2020

Keywords:
EAF steel making slag
EAF steel making dust
Zn
Alkali activation

ABSTRACT

Steel production in electric arc furnaces yielding formation of two waste materials, toxic electric arc furnace dust (EAFD) and non-hazardous electric arc furnace slag (EAFS). EAFD presents a potential hazard to the environment as it is characterized by the presence of heavy metals. This study dealt with the synthesis and characterization of alkali activated slag cement (AAS) based on EAFS with addition of 1-7% of Zn-rich EAFD dopant. Effects of slag replacement with dust on the compressive strength, physico-chemical, mineralogical and morphological properties of AAS cement were evaluated. This replacement lead to the development of porosity of AAS matrix, and retardation of slag alkali activation which resulted in the weakening of the AAS structure and hence in compressive strength decrease as pure AAS cement compressive strength was 21.04 MPa while AAS doped with 7% of EAFD reached only 8.4 MPa. On the other hand, AAS doped with 5% of EAFD exhibited compressive strength of 13.82 MPa, making it is still suitable for construction purposes... Scanning electron microscopy coupled with energy dispersive X-ray spectroscopy (SEM/EDS), scanning transmission electron microscope (STEM) in high angle annular dark field (HAADF) mode, X-ray powder diffraction (XRPD) investigations and standard EN 12457-2 leaching test provided information on the ability of AAS based on EAFS to fix Zn in AAS matrix.. The concentration of Zn in leachate of AAS cement doped with 5% of EAFD was 9.20 mg/kg which is below the limit prescribed for the granular waste acceptable at non-hazardous landfills according the European Directive 2003/33/CE.

* *Corresponding author.*
E-mail: irena@ucg.ac.me (I. Nikolić).

https://doi.org/10.1016/j.jmrt.2020.09.024

1. Introduction

It is well known that, in the process of steel production, via electric arc furnaces, two by-products are formed and are generally accepted as waste materials, one being non-hazardous - electric arc furnace slag (EAFS) and the other being the hazardous electric arc furnace dust (EAFD). The former is mainly consist of oxides of metals such as calcium, iron, silicon, aluminium and manganese, while the latter is mainly comprised of iron and zinc oxides, but depending on the composition of scrap charged into electric arc furnace, the presence of other heavy metals, to a lesser extent, was also observed [1]. The potential of these heavy metals to leach into the environment contributes to EAFD being classified as hazardous waste. Steel production in electric arc furnaces generates about 150–180 kg of EAFS and 20 kg of EAFD per tonne of steel produced [1,2]. Since the production of crude steel in the European Union was 162 million of tonnes in 2016, around 32 % of which was produced by electric arc furnace route [3], valorisation of steel making by-products is of great importance from a stand point of environmental protection. While about 85-90% of steelmaking slag is utilized in various industrial applications, recycling of hazardous dust is still at a low level [4].The primary interest for EAFD recycling is, naturally, the recovery of valuable metals - iron and zinc. Generally, this can proceed via pyro- and hydrometallurgical processes. Pyrometallurgical processes are based on the carbothermic reduction of metal oxides present in EAFD [5]. Although some of them have found commercial applications, they generally suffer from the problem of high energy consumption which is why hydrometallurgical treatments is a preferable method for metal recovery from EAFD. These processes are mainly focused toward the valorisation of Zn as it is a valuable metal with the highest content in EAFD. Although they are more favourable from the standpoint of energy consumption, dissolution of undesired metal species, especially iron, requires additional methods for solution purification [6]. Moreover, the efficiency of Zn recovery by hydrometallurgical treatment is dependent on the mineralogical form of Zn present in EAFD i.e. only Zn present in the form of zincate (ZnO) phase can be easily dissolved in acid or alkaline solutions while Zn present in the form of zinc ferrite ($ZnFe_2O_4$) cannot be easily leached out in the same manner. Other alternative routes of EAFD management involve fixation of toxic heavy metals present in EAFD by vitrification and stabilization/solidification process. Vitrification decreases the release of toxic components from EAFD by their immobilization into a glass network [7–9]. However, high energy consumption is a limiting factor for commercial applications of this process. An alternative is the low-cost stabilization/solidification which enables chemical fixation or physical encapsulation of toxic components from EAFD and/or transformation of EAFD into a stable, less permeable material, with low toxic component release.

Cement binder is widely used for stabilization/solidification of various kinds of toxic waste, including EAFD [10–12]. The efficiency of the process has been evaluated through the compressive strength and leaching tests of stabilized/solidified product i.e. heavy metals release from stabilized/solidified product in contact with various leaching solutions and compliance with prescribed leachate limits. It has been reported that EAFD addition to cement lead to the decrease of strength of stabilized/solidified product in comparison to the hardened neat cement paste [11,12]. Thus, a proper amount of added EAFD is required to obtain a monolith with satisfactory compressive strength that would enable its manipulation and avoid or reduce the risk of fracture. In general, it has been shown that the cement matrix can fix heavy metals present in EAFD but stabilization/solidification using cement as the sole binder is not sufficient to ensure the release of some heavy metals below the prescribed legal limit values and convert the EAFD into a non-hazardous form [11]. Release of heavy metals from EAFD stabilized/solidified in cement matrix can be reduced by the addition of certain additives. Salihoglu and Pinarli [13] have reported that lime addition to the mixture of cement and EAFD reduced Zn and Pb leachability with an optimum composition of 30% EAFD/35% lime/35% cement was proposed in order to met the landfill criteria for non-hazardous waste. Moreover, partial substitution of cement binder with ground granulated blast furnace slag (GGBFS) positively affected heavy metals retention into the stabilized/solidified product [14].

There has been significant progress in terms of stabilization/solidification of EAFD using alternative binders instead of cement. Laforest and Duchesne have reported that GGBFS is more effective than ordinary Portland cement (OPC) in retaining heavy metals from EAFD [14]. Pereira et al. [15] have shown that objectives of EAFD solidification/stabilization by using fly ash as a main binder were easily achieved in regards the compressive strengths of solidified/stabilized product while the Pb, Zn, Cr and Cd concentration limits were not exceeded in leachates when the final pH of leachate was within a range of values corresponding to the minimum solubility of the metals in the leaching medium.

Stabilization/solidification of EAFD using geopolymerization technology has also proposed. Pereira et al. [16] have reported that fly ash based geopolymers have the potential to fix Zn, Pb, Cd and Cr from EAFD and that mechanical properties and heavy metals release from EAFD stabilized/solidified in fly ash based geopolymers in general are more favourable than those achieved by stabilization/solidification using cement binder. Nikolić et al. [17] pointed out that increase of EAFD content in fly ash based geopolymers lead to the decrease of compressive strength when compared to reference geopolymer and that geopolymers with 10% addition of EAFD are relatively stable in neutral and alkali environment, while in the pH range of 2–5.5 solubility of Zn and Pb is a concern for this type of materials [17]. According to Arnold et al. [18] fly ash based geopolymers with 5% of EAFD did not exhibit a change in compressive strength compared to the reference geopolymer while additions of up to 20% of EAFD were classified as non-hazardous materials with respect to leachability of heavy metals.

On the other hand, EAFS is mainly utilized in civil engineering: in asphalt mixtures [19] for road construction [20] and concrete production [21–23]. However, these studies considered the application of EAFS without decreasing the initial FeO content which is a limiting factor for the EAFS use as supplementary cementitious materials. The FeO content in EAFS can be reduced by a two-stage reduction process that

Table 1 – Chemical composition of EAFS and content of metals in EAFD.

EAFS[a]		EAFD[b]	
Component	%	Component	%
CaO	45.9	Fe	21.7
FeO	23.5	Ca	2.30
SiO_2	12.2	Si	6.47
Al_2O_3	7.2	Al	0.25
MgO	6.5	Ti	0.14
MnO	1.3	Zn	28.3
TiO_2	1.06	Pb	3.15
Fe_2O_3	0.9	Cr	0.52
Cr_2O_3	0.8	Cd	0.11
CaO (free)	0.6	Cu	0.53
		Ba	0.15
		Mn	2.21
		Mg	1.50
		Mo	0.31
		Na	0.44
		Ni	0.12

[a] Chemical composition of slag provided from the steelmaking company.
[b] Non-normalized chemical composition of EAFD determined by ICP-OES after microwave assisted digestion of the samples. Results indicate the mean value obtained from three parallel samples (RSD of measurement less than ±3%).

includes an Al-dross reduction reaction followed by direct carbon reduction yielding the final FeO content in modified EAFS below 5 wt%, compatible with cement clinker applications [24]. Moreover, the content of FeO present in EAFS in the form of magnetite can be reduced by silica addition with the aim of precipitating FeO and leaving a low-basicity matrix that can be readily cooled into an amorphous phase, favorable for utilization in the cement industry [25]. The usage of this slag for the synthesis of alkali activated slag (AAS) cements is also addressed [26]. Alkali activated slag cement or ġreen cements; produced by means of chemical reaction of solid raw material with alkaline activator (solution of MOH or M_2SiO_3 were M is Na or K ion), displayed different properties depending on the raw material selection [27]. The first step in the production of AAS cements is simultaneous hydrolysis and dissolution of slag in a highly alkaline solution which is accompanied by the destruction of Ca—O, Mg–O, Al–O–Si and Si–O–Si bonds from the slag. The result is formation of monomeric $Si(OH)_4$ and $[Al(OH)_4]^-$ species which further react with the OH^- ions from alkali solution and to produce complexes $[(HO)_4\text{-}xSiO_x]^{-x}$ and $[AlO(OH)_3]^{2-}$. The second step is polycondesation of these species and reaction with Ca^{2+} ions yielding reaction product of slag alkali activation – amorphous calcium aluminate silicate hydrate (C-A-S-H) gel [28–30]. The last step is hardening of C-A-S-H gel by curing at ambient or elevated temperatures.

The purpose of these study was to investigate the use of alkali activated cement based on EAFS as an agent for a stabilization/solidification of EAFD. Alkali activated slag

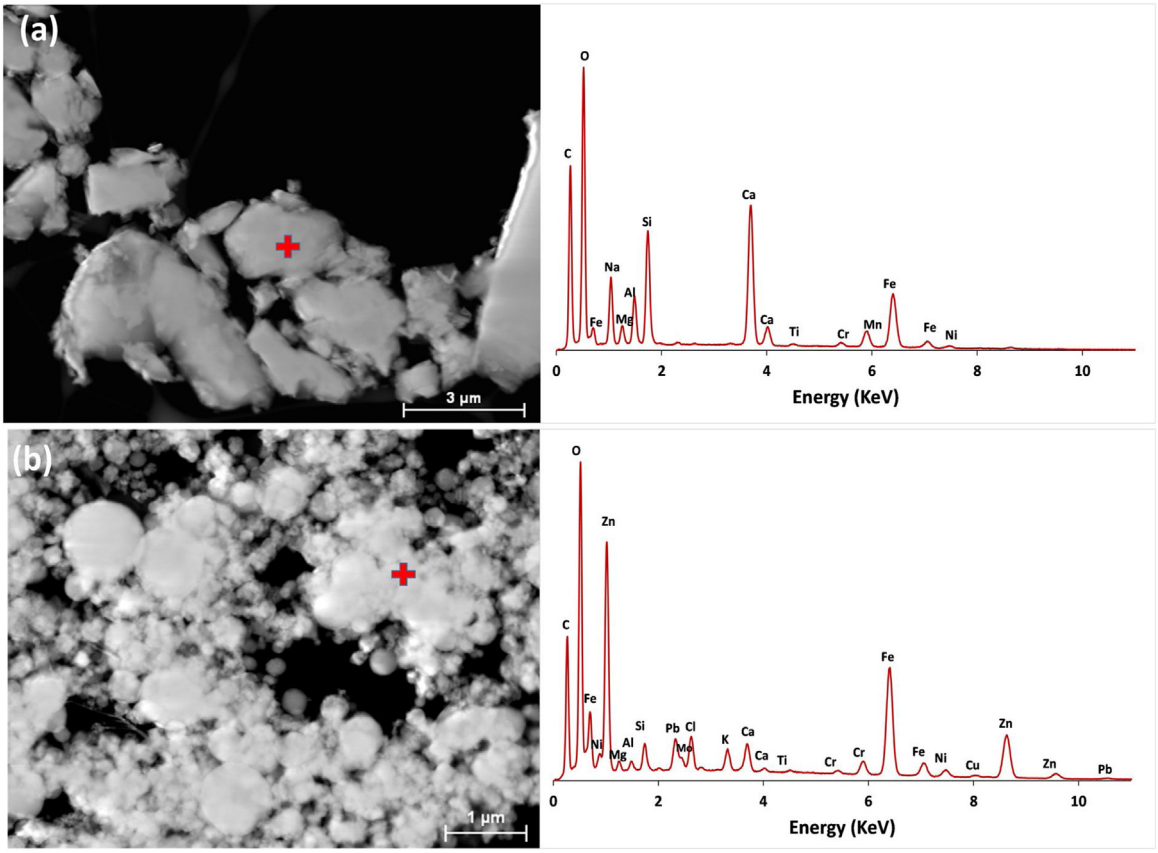

Fig. 1 – Scanning electron micrographs along with corresponding EDS spectra taken from area marked with red cross of (a) EAFS and (b) EAFD samples.

Table 2 – Physical properties of EAFS and EAFD (Standard deviation is given in parenthesis).

Parameter	EAFS	EAFD
Pore volume, (cm^3/g)	0.000182	0.007121
Average pore diameter, (nm)*	12.88 (±9.1%)	18.03 (±12.9%)
Average particle size, (μm)**	9.67 (±1.2%)	14.68 (±0.8 %)

cements based on EAFS doped with Zn-rich EAFD were synthesized. The effect of EAFD addition on the mechanical, physico-chemical, mineralogical and morphological properties of alkali activated slag cement was discussed with an emphasis on the immobilization of Zn in the alkali activated slag matrix.

2. Experimental

2.1. Materials

Steel Mill Nikšić in Montenegro provided EAFS and EAFD used in this investigation and their chemical compositions are given in Table 1. Since EAFS was produced in the form of big pieces, for the purpose of alkali activation process, it was ground down to a fine powder while EAFD powder was used as produced. The microstructures of EAFS and EAFD accompanied with elemental distribution within samples are given in Fig. 1 and their physical properties are given in Table 2 and Fig. 2. Ground EAFS particles are characterized by irregular shape, as shown in Fig. 1(a), with pore volume of 0.000182 cm^3/g and average pore width of 12.88 nm (Table2). On the other hand, EAFD particles are agglomerates of sphere like particles as noted in Fig. 1(b) with pore volume and average pore width of 0.007121 cm^3/g and 18.03 nm, respectively (Table 2). Both, EAFS and EAFD show a narrow particle size distribution (*span* = 2.038 for EAFS and *span* = 2.031 for EAFD) with average particle size of 9.67 (±1.2%) μm for EAFS and 14.68 (±0.8%) μm for EAFD, while 90% of particles are smaller than 23.61 μm and 35.54 μm, for EAFS and EAFD, respectively (Fig. 2).

2.2. Synthesis

The sample of alkali activated slag (AAS) cement was prepared by mixing EAFS with alkali activator in a mass ratio of 4:1, which was in this case Na_2SiO_3 solution, prepared by mixing 10 M of NaOH and commercial water glass (Na_2O = 8.5%, SiO_2 = 28.5%, density of 1.4 kg/m^3) in a mass ratio of 1.5:1 for 10 min. A paste prepared in such a way was cast into a cylindrical plastic mould (50 × 100 mm), sealed with a lid to prevent the loss of evaporating water and cured in the oven for 48 h at 65 °C. Subsequently, the specimens were removed from moulds and left to stay an additional 28 days at ambient temperature. The samples of alkali activated slag cement doped with EAFD were prepared by replacing 1, 3, 5 and 7 % of the total amount of slag with EAFD and denoted as S/D-1, S/D-3, S/D-5 and S/D-7, respectively. The choice of slag replacement with EAFD (1–7 %) was based on preliminary tests. For this purpose, EAFD was initially mixed with NaOH solution for 10 min in order to allow leaching of Zn and other heavy metals from EAFD and subsequently the Na_2SiO_3 solution was added with continual mixing for 5 min. Finally, EAFS was added and the obtained paste was mixed for an additional 10 min followed by same curing regime as for the AAS sample.

2.3. Characterization

Particle size of EAFS and EAFD was determined using a laser particle size analyser (Mastersizer 2000, Malvern Instruments Ltd., United Kingdom). For this purpose, EAFD and powdered EAFS were mixed with distilled water in an ultrasonic bath for 5 min.

Unconfined compressive strength testing of hardened AAS and S/D samples was done in triplicate at a strain rate of 1 mm/min using the mechanical press CMT 4000, China. Prior to testing, the surfaces of the sample were polished flat and parallel.

Porosity of samples was evaluated using N_2 adsorption/desorption isotherms, measured using the ASAP 2020 instrument. To ensure the removal of moisture, degassing of both samples was performed at 100 °C for 24 h. Pore size distribution, pore volumes and average pore diameter were determined with the Barret–Joyner–Halenda (BJH) method [31].

Thermogravimetric and differential thermal analysis (TGA/DTA) measurements were performed using the TA-SDT 2060 instrument. Finely ground 20 mg of the sample was placed in a platinum crucible and heated to 1150 °C at a constant heating rate of 15 °C/min.

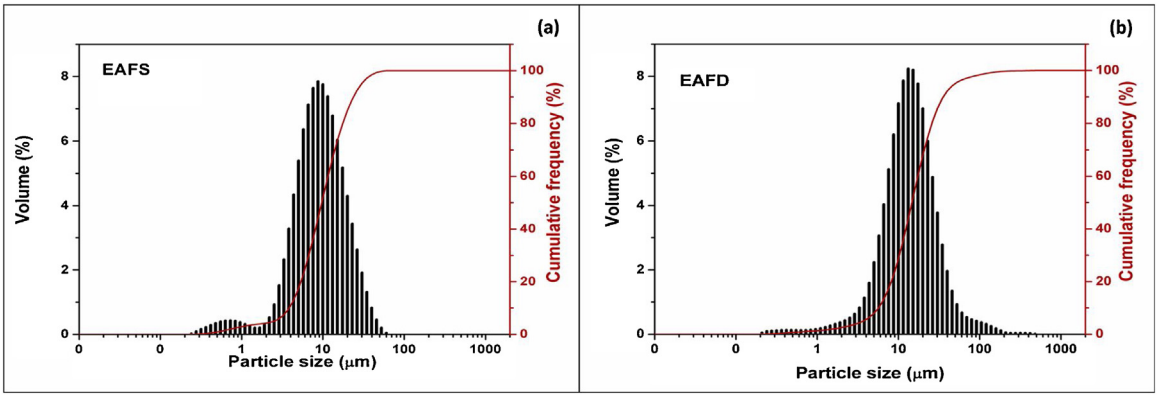

Fig. 2 – Particle size distribution of (a) EAFS and (b) EAFD based on particle number and cumulative percentage frequency.

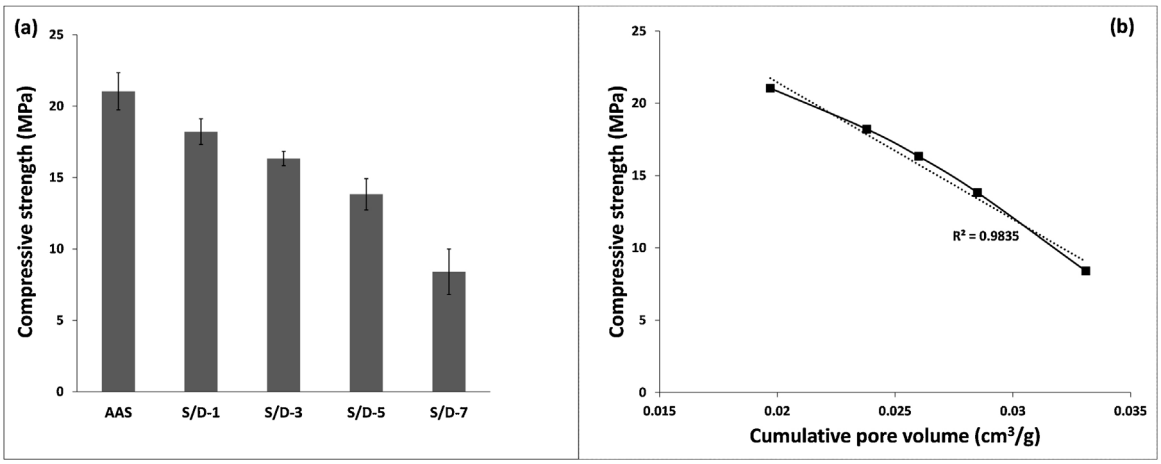

Fig. 3 – (a) Compressive strength of control AAS and S/D samples and (b) Compressive strength versus pore volume of AAS and S/D samples.

Table 3 – Porosity of control AAS and S/D samples.

Sample	AAS	S/D-1	S/D-3	S/D-5	S/D-7
Cumulative pore volume (cm^3/g)	0.019701	0.023762	0.026007	0.028529	0.033051

Phase composition of source materials and the samples of alkali activated slag cement (with and without EAFD addition) was performed by X-ray powder diffraction (XRPD) technique. The data was collected on a Rigaku RINT-TTRIII diffractometer, with Cu-Kα radiation of $\lambda = 1.5406$ Å at room temperature in the 2θ range of 10–70° with a scanning step of 0.02° and scan speed of 5 s per step.

Fourier transform infrared (FT—IR) spectra were recorded on a Thermo Scientific™ Nicolet™ iS™10 FT—IR Spectrometer equipped with attenuated total reflectance (ATR) accessory. The ATR/FT—IR measurements were done at room temperature in the 400–4000 cm^{-1} wavelength interval, with a resolution of 4 cm^{-1}.

Microstructural investigations were carried out using the FEI Helios NanoLab 660 SEM/FIB dual beam system, equipped with the EDAX energy dispersive X-ray spectrometer (EDS) and FEI TITAN Themis^3 300 scanning transmission electron microscope (STEM) in high angle annular dark field (HAADF) mode, equipped with the Super-X energy dispersive X-ray spectrometer (EDS) with Bruker Esprit software.

The impact of the EAFS, EAFD, AAS and S/D samples on the environment is assessed using the Compliance Leaching Standard Test EN 12457-2 proposed in the European Directive on the Landfill of Waste, 2003/33/CE [32]. This test is used to determine whether the waste complies with specific reference values collected in 2003/33/CE Directive. Council Decision 2003/33/EC established limit values for the acceptance of granular wastes at landfills for inert, non-hazardous or a hazardous waste. For the purpose of EN 12457-2 test the powdered solid was mixed with deionized water in a solid to liquid ratio of 1:10. After 24 h the suspension was filtrated and metal content in eluate was determined using inductively coupled plasma optical emission spectrometry (ICP-OES) and compared with the limits established by the European Directive 2003/33/CE [32].

3. Results and discussion

3.1. *Compressive strength and porosity*

Stabilization/solidification of EAFD into slag based alkali activated slag cement lead to the change of mechanical properties of AAS. Unconfined compressive strength of S/D products is greatly dependent on the percentage of slag replaced with dust (Fig. 3(a)) and it is evident that this replacement lead to the deterioration of mechanical properties of AAS. The control AAS sample exhibited compressive strength of 21.04 MPa while the addition dust (1-7%) lead to continual strength decrease i.e. S/D samples with 1-5% of EAFD exhibited strength above 10 MPa which is suitable for both, landfill and construction applications where values above 0.35 MPa and 10 MPa, respectively, are required [33,34] while the S/D sample with 7% of EAFD reached a compressive strength of 8.4 MPa, which makes it suitable for landfill purpose only.

The decrease strength of AAS cement with an increase of dust content is ascribed to the decrease of cumulative pore volume (Table 3). Moreover, the mechanical properties of AAS cements are dependent on the properties of reaction product of slag alkali activation (C-A-S-H gel) [35]. However, the plot of compressive strength versus pore volume (Fig.3(b)) is almost linear with the regression of $R^2 = 0.9835$ which indicates that in this case porosity preferably influences the strength of AAS cement containing the EAFD. Decrease of compressive strength of AAS cement with EAFD addition is attributed to the change of porosity in the structure. The curves of pore size distribution of both samples, pristine EAFS and EAFD indicate a bimodal pore size distribution with significant difference in pore volume (Fig.4(a)). The two peaks that reflect the two different pore systems were observed in both samples, smaller around 18.5 nm and 28 nm for EAFS and EAFD, respectively and

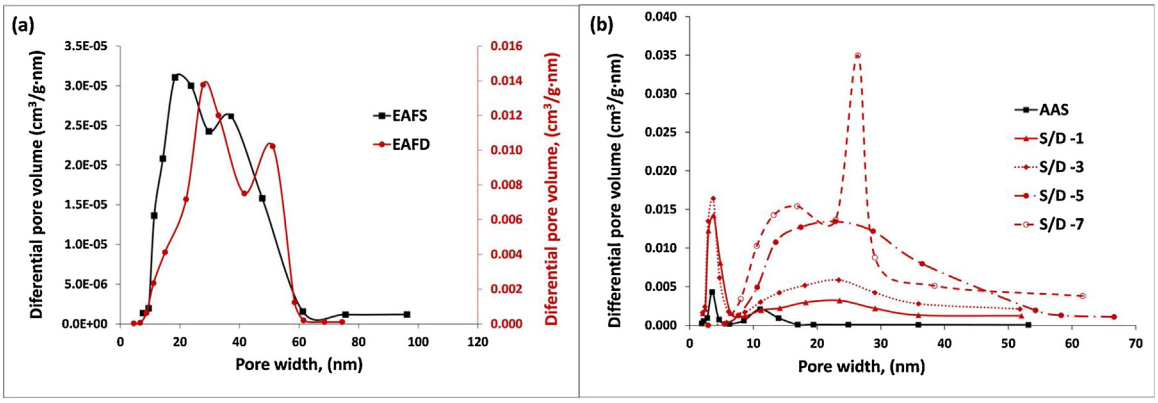

Fig. 4 – Pore size distribution of (a) EAFS and EAFD (a) and (b) AAS and S/D samples.

larger around 33.0 nm 51.2 nm for EAFS and EAFD, respectively. Since EAFD and EAFS used in this study had cumulative pore volumes of 0.007121 and 0.000182 cm^3/g, respectively (Table 2), i.e. EAFD had an one order higher cumulative pore volume, replacement of slag by EAFD lead to the continual increase the porosity of final S/D products (Table 3). Pore size distribution of control AAS and S/D samples are given in Fig.4(b). The pore size distribution of AAS sample is characterized by two peaks which note that the width of the majority of pores to be around 3.5 and 11.0 nm. After 1% and 3% addition of dust, the differential curves of pore size distribution indicate bimodal pore size distributions. The narrow region that reflects the smaller pore systems (with maximum around 3.7 nm) was still present in both, S/D-1 and S/D-3 samples. However, the broad regions with the maximum at around 23.5 nm were also observed which indicates that EAFD addition leads to the development of larger pore sizes. Moreover, the S/D-3 sample displayed a higher pore volume in comparison to S/D-1 sample. The broadening of the peak with a maximum at around 23.5 nm and increase in pore volume were observed with the addition of 5% of EAFD while 7% addition of EAFD further increased the pore volume and split the single pore system into the bimodal with pore sizes mostly around 13.2 and 26.4 nm. Since the sample of alkali activated slag cement with 5% of EAFD exhibited mechanical properties required in potential construction applications, further investigations were focused on the control AAS and S/D-5 samples.

3.2. *X-ray powder diffraction (XRPD)*

The results of XRPD analysis are shown in Fig. 5. The main crystal phases identified in EAFS sample were larnite, Ca_2SiO_4 (COD ID 96-901-2790), wüstite, FeO (COD ID 96-101-1199), gehlenite, $Ca_2Al(AlSiO_7)$ (COD ID 96-100-0049), and montcellite, $CaMgSiO_4$ (COD ID96-900-1081), while spinel, $MgAl_2O_4$ (COD ID 96-900-2745) and calcite, $CaCO_3$ (COD ID 96-901-6180) phases were also present in smaller quantities. Crystal phases of EAFD were elucidated to be franklinite, $ZnFe_2O_4$ (COD ID 96 -901-2442), zincite, ZnO (COD ID 96-901-1663) and magnetite, Fe_3O_4 (COD ID 96-900-6922).

The percentage of crystalline, i.e. the amorphous phase in the samples were estimated as relationship between total area of the crystalline fraction and the sum of areas of crystalline

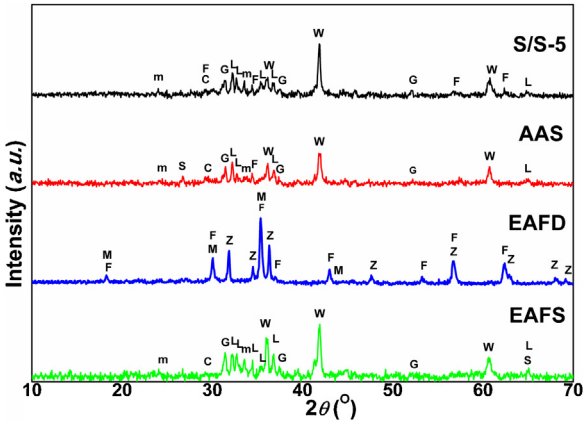

Fig. 5 – Diffractograms of EAFS, EAFD, AAS and S/D-5 products.

and amorphous fractions, calculated using JADE software. The obtained results showed crystallinity of 58.8% for AAS and 55.6 % for S/D-5 sample. Accordingly, the content of amorphous phase in AAS and S/D-5 sample was 41.2 % and 44.4 %, respectively.

The presence of undissolved species: larnite, gehlenite, wuestite, montcellite and calcite, as residues from undissolved slag, was observed in the AAS sample. Additionally, the presence of franklinite, originating from unreacted EAFD was observed in the S/D-5 sample. From a standpoint of fixation of toxic component from EAFD into the S/D matrix, it is important to notice the absence of zincate in the S/D sample which indicates its dissolution during the alkali activation and its participation in the amorphous phase

3.3. *Fourier transform infrared (FTIR) spectroscopy*

The FTIR spectra of source materials (EAFS, EAFD), control AAS and S/D-5 samples are given in Fig. 6. The most important bands in the FTIR spectrum of EAFS were observed at 495 cm^{-1} ascribed to O-T-O bending modes of TO_4 tetrahedra (T = tetrahedral Si or Al) [36] and in the 750 –1200 cm^{-1} region, ascribed to stretching vibrations of Al—O—Si and Si—O—T bonds [37–39]. The band at 1473 cm^{-1} is attributed to vibra-

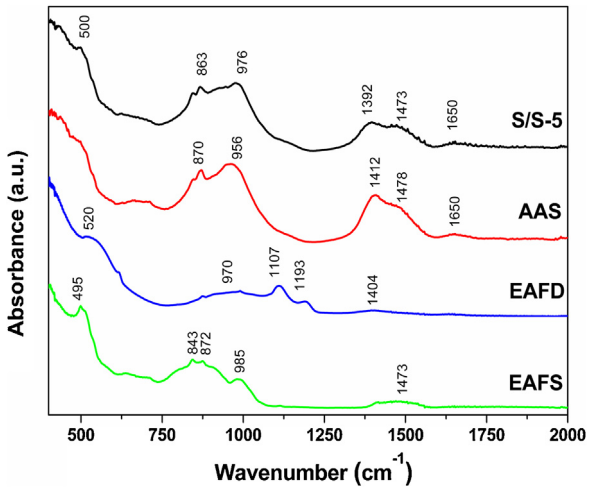

Fig. 6 – FTIR spectra of EAFS, EAFD, AAS and S/D-5 products.

tional modes of CO_3^{2-} ion. The spectrum of EAFD exhibits a band at 520 cm^{-1} ascribed to Zn—O bonds [40] and bands between 930 and 1100 cm^{-1} can be assigned to Si—O vibrations [41]. Moreover, bands at 1193 cm^{-1} and 1404 cm^{-1} ascribed to SO_4^{2-} and carbonate ion (CO_3^{2-}) vibrations, respectively, were observed. Spectrum of control AAS sample exhibits a band at 965 cm^{-1} associated with stretching Si–O vibrations in the SiO_4 tetrahedra that comprise the calcium aluminate silicate hydrate (C-A-S-H) gel [42]. Moreover, the peak ascribed to O—T—O bending modes of TO_4 tetrahedra at 495 cm^{-1} shows a decrease in intensity and a shift to a higher wavelength (500 cm^{-1}), in comparison with the spectra of EAFS, which is related to the slag dissolution and formation of C-A-S-H gel during the alkali activation process. The replacement of slag with EAFD in the alkali activation process results in shift of the band, ascribed to the C-A-S-H gel, to higher wavelengths (976 cm^{-1}) indicating Zn incorporation into C-A-S-H phase [43]. Moreover, compared to EAFD spectrum, the decrease in intensity of bands related to Zn-O bond was observed. These changes are related to the ZnO dissolution in alkali environment during the alkali activation process and Zn incorporation in the reaction product of slag alkali activation [43]. Moreover, both, AAS and S/D-5 samples displayed bands at 1650 cm^{-1}, attributed to the vibrations of OH groups from water molecules. The presence of vibrations assigned to CO_3^{2-} were observed in both, AAS (at 1412 cm^{-1} and 1478 cm^{-1}) and S/D-5 (at 1392 cm^{-1} and 1473 cm^{-1}).

3.4. *Scanning electron microscopy and scanning transmission electron microscopy in tandem with energy dispersive X-ray spectroscopy*

Morphology of control AAS and S/D-5 samples was examined using scanning electron microscopy (SEM) as well as scanning transmission electron microscopy (STEM) in high angle annular dark field (HAADF) mode, both in tandem with energy dispersive X-ray spectroscopy (EDS), the results of which are given in Figs. 7 and 8. Microstructure of control AAS sample (Fig. 7a) is characterised by the presence of a dense well-

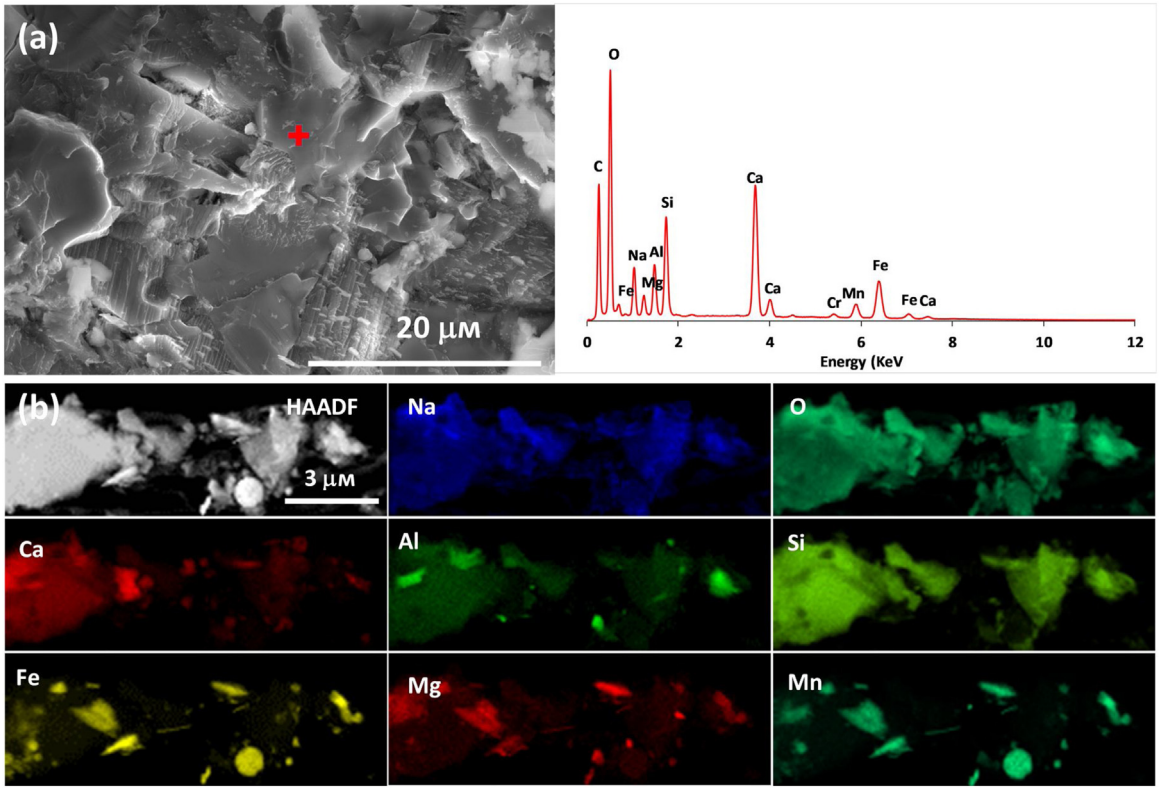

Fig. 7 – (a) SEM micrograph of AAS with EDS point spectrum taken from area noted by red cross in SEM image and (b) HAADF STEM micrograph of AAS with EDS maps noting elemental distribution within sample.

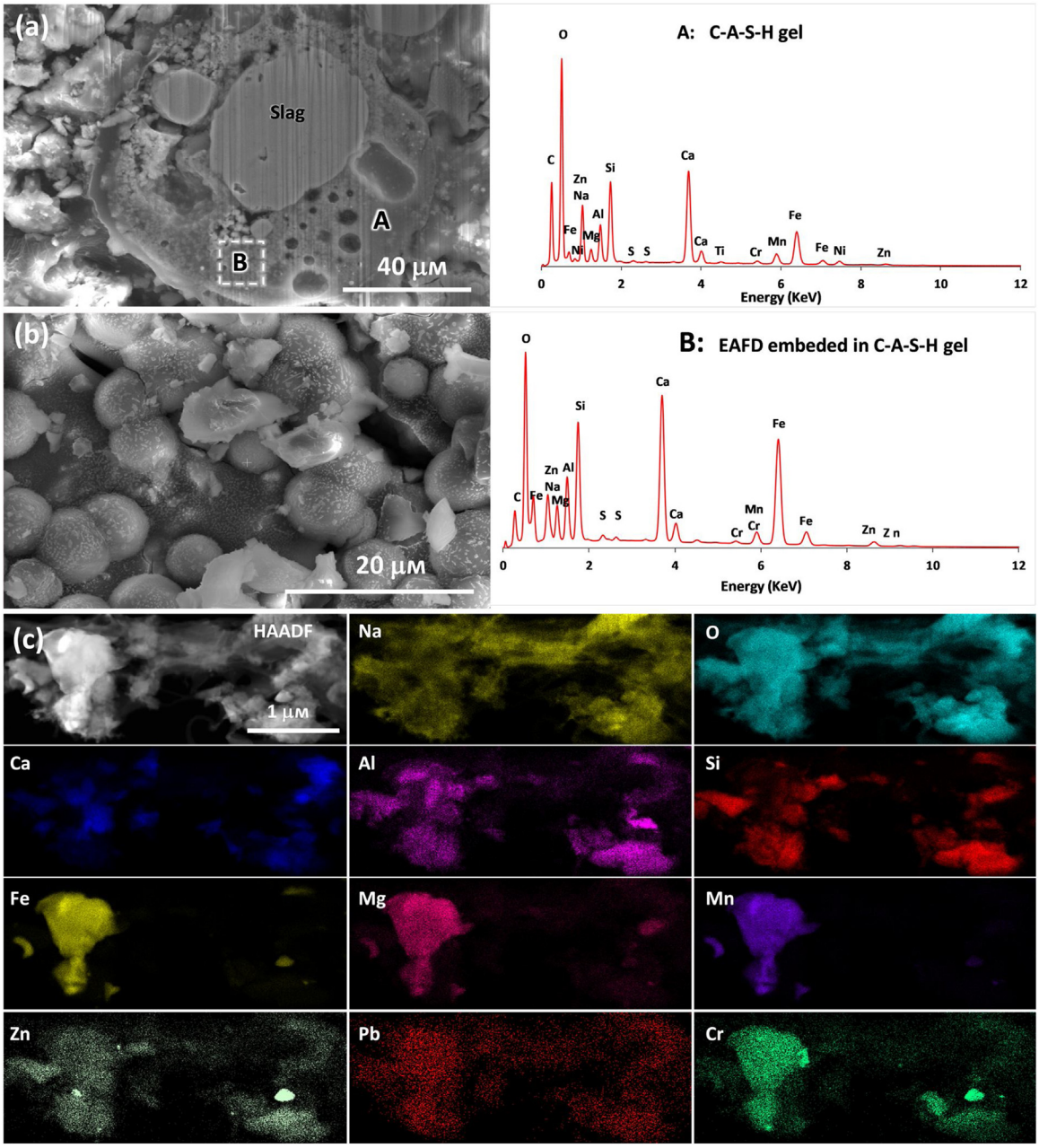

Fig. 8 – (a) SEM micrograph of S/D-5 and EDS spectrum taken from area "A" noted in SEM; (b) High magnification SEM of area "B" noted by white dashed rectangle in SEM in (a) and EDS spectrum taken from same area (c) HAADF STEM micrograph of S/D-5 with EDS maps noting elemental distribution within sample.

developed structure of C-A-S-H gel. EDS spectrum taken from C-A-S-H gel region (noted by red cross in Fig. 7 (a)) reveals high content of Ca and Si and much lower Al content which is typical for C-A-S-H phase [44]. Images obtained by STEM/HAADF along with appropriate EDS maps indicate the homogenous nature of C-A-S-H gel since the Ca, Si and Al distribution is overlapping (Fig. 7b). Moreover, EDS maps also indicated the presence of unreacted slag particles in the structure, bounded in the reaction product of slag alkali activation, as the Fe and Mn distribution is overlapping i.e. Fe and Mn are concentrated in the same areas within the sample (Fig. 7b).

Replacement of slag by EAFD in the order of 5% resulted in a more porous and heterogeneous structure (Fig. 8(a)), consisting of a product of alkali slag activation reaction i.e. C-A-S-H gel (area A) containing trapped unreacted EAFD particles (area B). According to EDS spectrum taken from area A, fixation of Zn in S/D-5 product occurs via chemical immobilization since the presence of Zn was detected in the EDS spectrum of C-A-S-H gel (Fig.8(a)). This is also confirmed by HAADF STEM/EDS analysis (Fig. 8(c)) where EDS maps clearly show that Ca, Si, Al and Zn are distributed in the same areas which indicates that Zn is chemically incorporated in reaction product of slag

alkali activation. Moreover, Cr and Pb seem to be concentrated in the same areas, which could indicate that all heavy metals in EAFD follow the same immobilization mechanism although their low content did not allow for a more in depth discussion.

To promote the chemical immobilization and incorporation of Zn in the reaction product of slag alkali activation (C-A-SH gel) EAFD was initially mixed with NaOH solution to allow Zn dissolution from EAFD and to react with species present in the reaction medium of alkali activated system. Incorporation of Zn in C-A-S-H gel may follow the next pathway [45]: dissolution of Zn in NaOH results in a formation of zincate $[Zn(OH)_4]^{2-}$ (Eq. 1) which further reacts with calcium ions provided by the slag dissolution in alkali activator yielding calcium zincate phase $Ca(Zn(OH)_3)_2 \cdot 2H_2O$ (Eq. 2)

$$Zno_{(s)} + 2OH^-_{(aq)} + H_2O_{(l)} \rightarrow Zn(OH)^{2-}_{4(aq)} \quad (1)$$

$$2Zno(OH)^{2-}_{4(aq)} + Ca^{2-}_{(aq)} + 2H_2O_{(l)} \rightarrow Ca(Zn(OH)_3)_2 \cdot 2H_2O_{(s)} + 2OH^-_{(aq)} \quad (2)$$

In a reaction medium of alkali activated solution, reaction between calcium ions and aluminium and silica species also occurs yielding C-A-S-H gel. The calcium ions are consumed preferentially into the calcium zincate phase as long as there is zinc available. Formation of C-A-S-H gel occurs when the whole of dissolved zinc is consumed in calcium zincate phase. When the C-A-S-H phase begins to form, calcium zincate phase dissolves in C-A-S-H phase since C-A-S-H gel is thermodynamically more stable than calcium zincate phase [45].

Since XRPD analysis did not show the presence of ZnO in stabilized/solidified sample (S/D-5 sample), it can be concluded that all of ZnO present in EAFD was dissolved under the conditions that we set in this experiment and that Zn originated from ZnO is incorporated in C-A-S-H gel as shown by SEM/EDS analysis (Fig. 8 (a)).

Another mechanism of Zn incorporation in C-A-S-H gel is also proposed. It is based on the reaction of dissolved Zn with silica species present in the reaction medium of alkali activated systems leading to the formation of insoluble zinc silicate phase (Eq. 3) [46]. Reaction product of slag alkali activation in the presence of Zn is probably a mixture of zinc silicate gelatin and amorphous C-A-S-H gel [43].

$$Zn(OH)^{2-}_{4(aq)} + \left[H - OSiO_x(OH)_{3-x}\right]^{x-}_{(aq)} \rightarrow \left[(OH)_3ZnOSiO_x(OH)_{3-x}\right]^{(x+2)-}(aq) + H_2O_{(l)} \quad (3)$$

Concerning area B, EDS spectrum (Fig. 8(b)), in addition to C-A-S-H gel, reveals a high content of Fe and the presence of Zn and other heavy metals, typical for an EAFD composition. This evidence indicates that stabilization/solidification of EAFD occurs via physical encapsulation as well as chemical immobilization of Zn in stabilized/solidified (Fig. 8(b)) remained in undissolved EAFD which is in the form of franklinite as shown by XRPD analysis.

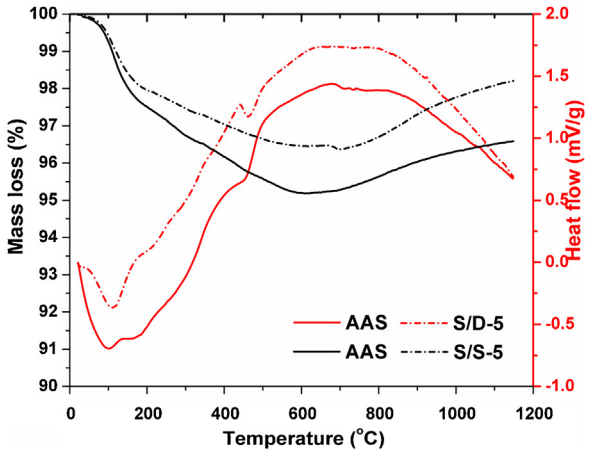

Fig. 9 – TG (black lines) / DTA (red lines) analyses of AAS and S/D-5 samples given as mass loss and heat flow, respectively, as a function of temperature.

3.5. *Thermogravimetry/Differential thermal analysis (TG/DTA)*

TG analysis is often used in order to estimate the extent of hydration e.g. the mass loss up to 600 °C is a measure of hydration degree [47]. Higher mass loss indicates a higher amount of hydration product (C-A-S-H) in alkali activated slag cement [48]. TG/DTA curves of AAS and S/D samples are given in Fig. 9. TG curves of both, AAS and S/D-5 samples showed mass loss up to 600 °C, attributed to the evaporation of physically adsorbed water from C-A-S-H gel up to 160 °C and thermal dehydration of this phase in the range of 160-600 °C [47,49]. The endothermic peaks in DTA curves of both samples around 100 °C imply the presence of C-A-S-H gel [50]. The mass loss on the TG curve of AAS sample up to 600 °C was ~4.7 % while the mass loss of S/D-5 sample was observed to be ~3.6% indicating the retardation effect of EAFD addition on the formation of reaction product of slag alkali activation. Zinc retards the formation of reaction product of slag alkali activation by forming metastable calcium zincate phase in the initial stage of alkali activation and depleting the Ca ions that are needed for nucleation and growth of the C-A-S-H gel [45]. In such a way, formation of C-A-S-H phase is delayed until all of the dissolved Zn is consumed for formation of calcium zincate phase [45].

3.6. *Leaching behaviour of S/D product*

The amount of detected metals leached out from EAFS, EAFD, AAS and S/D-5 samples by application of EN 12457-2 leaching test and criteria for the waste acceptance in landfills established by the European Directive 2003/33/CE [32] are given in Fig. 10. All samples generate alkaline leachates upon the completion of leaching tests. The pH values of leachates collected after the leaching of source materials were 10.95 for EAFS and 9.75 for EAFD sample while AAS and S/D samples generated highly alkaline leachates with similar pH values of 12.54 and 12.34, respectively.

The results have shown that the release of metals (Ba, Cr, Cu, Mo and Zn) from EAFS sample was below the criteria for

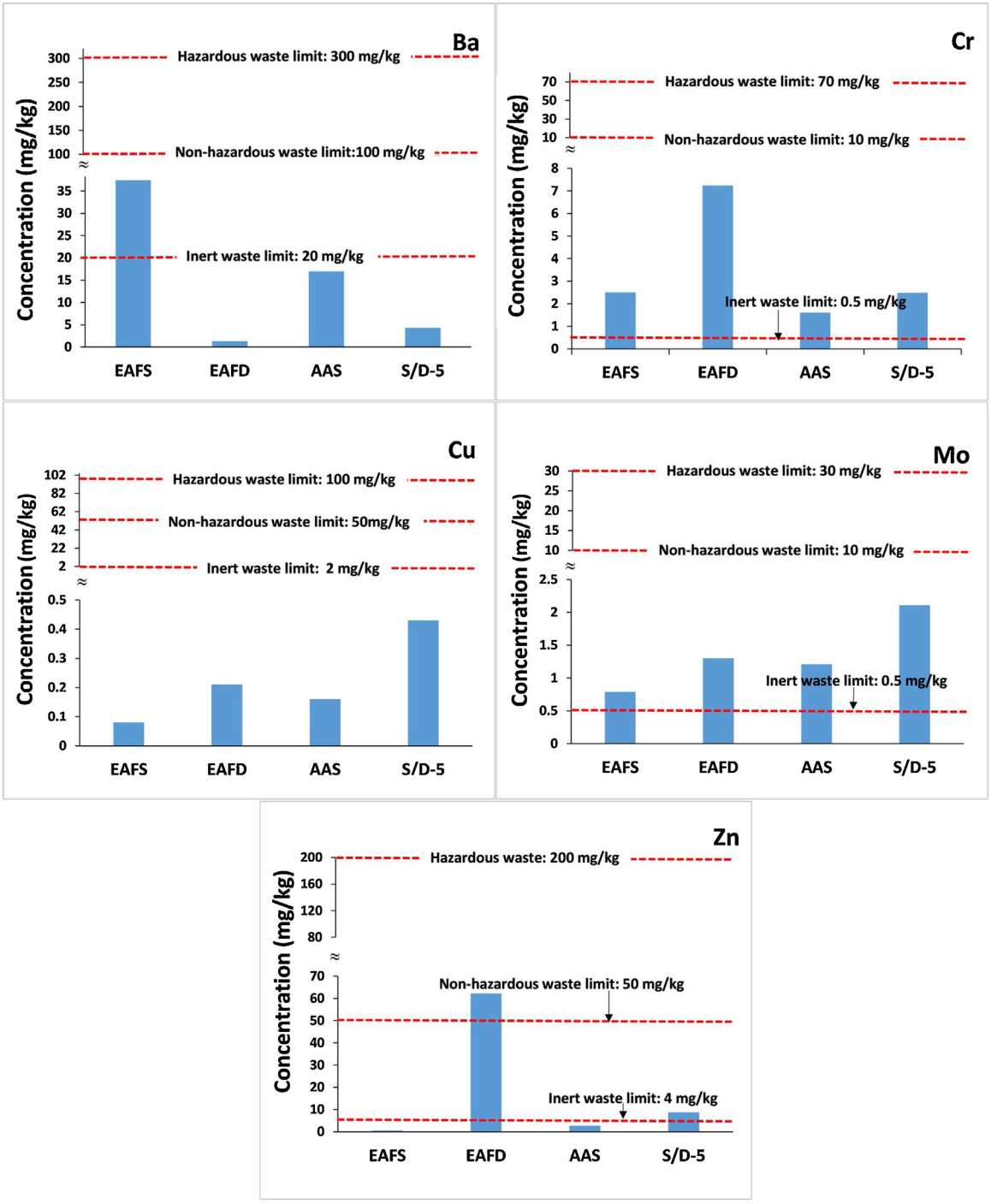

Fig. 10 – The results of EN 12457-2 leaching tests and maximal limits for granular waste acceptable at landfills (Inert, Non-hazardous and Hazardous); (Criteria established by the European Directive 2003/33/CE [32]).

waste acceptance in non-hazardous landfill. The amount of metals released from AAS sample also resulted in the classification of AAS sample as non-hazardous. However, the release of Zn from EAFD exceeded these limits. Obtained concentration of Zn in EAFD leachate was 62.18 mg/kg which excides the limits established for non-hazardous waste (4–50 mg/kg) i.e. EAFD is not allowed to be disposed of on landfills as non-hazardous waste but as hazardous waste. However, the sample of AAS cement containing 5% of EAFD was able to reduce the concentration of Zn (9.20 mg/kg) below the limit for non-hazardous waste which can be ascribed to the partial incorporation of metal into the reaction product of slag alkali activation (C-A-S-H gel) as showed by SEM/EDS analysis.

4. Conclusions

This research has been conducted in order to investigate effect of slag replacement with EAFD on the mechanical, physico-chemical, morphological and microstructural properties of

alkali activated slag cement. An environmental assessment of these materials has been made using the EN 12457-2 leaching test. Based on the results obtained, the following conclusion can be drawn:

- Slag replacement with EAFD lead to the deterioration of mechanical properties of alkali activated slag. Higher content of EAFD in S/D causes a more porous structure and loss of strength of S/D product in comparison to control AAS sample. Slag replacement with EAFD in the order of 5% enables potential use of S/D product in construction applications while the S/D product with higher amounts of EAFD met the criteria for landfill purposes.
- Slag replacement of EAFD has a retardation effect on the formation of C-A-S-H phase reaction.
- Fixation of EAFD into the AAS matrix occurred by chemical and physical immobilization. Chemical fixation of Zn into the reaction product of slag alkali activation (C-A-S-H phase) was confirmed by FTIR, SEM and HAADF STEM, the latter two coupled with EDS investigations.
- The leaching of Zn from S/D product is inferior in comparison to pristine EAFD and the S/D sample doped with 5% of EAFD met the criteria for granular waste disposal at landfills for non-hazardous waste according the EN 12457-2 test.

Conflicts of interest

The authors declare no conflicts of interest.

Acknowledgements

This work was supported by the Montenegrin Ministry of Science under grant no. 01-2383/2. VVR thanks the Ministry of Education, Science and Technological Development of the Republic of Serbia grant no. 451-03-68/2020-14/ 200287, VRR thanks the Serbian Academy of Sciences and Arts grant no. F141. The authors gratefully acknowledge the National Center for Electron Microscopy the Molecular Foundry, Lawrence Berkeley National Laboratory, which is supported by the U.S. Department of Energy under Contract # DE-AC02-05CH11231.

REFERENCES

[1] Sofilić T, Rastovčan-Mioč A, Cerjan-Stefanović Š, Novosel-Radović V, Jenko M. Characterization of steel mill electric-arc furnace dust. J Hazard Mater 2004;109:59–70, http://dx.doi.org/10.1016/j.jhazmat.2004.02.032.

[2] De Domenico D, Faleschini F, Pellegrino C, Ricciardi G. Structural behavior of RC beams containing EAF slag as recycled aggregate: numerical versus experimental results. Constr Build Mater 2018;171:321–37, http://dx.doi.org/10.1016/j.conbuildmat.2018.03.128.

[3] Euroslag 2016. https://www.euroslag.com/products/statistics/statistics-2016/ (accessed November 17, 2019).

[4] Lobato NCC, Villegas EA, Mansur MB. Management of solid wastes from steelmaking and galvanizing processes: a brief review. Resour Conserv Recycl 2015;102:49–57, http://dx.doi.org/10.1016/j.resconrec.2015.05.025.

[5] Lin X, Peng Z, Yan J, Li Z, Hwang JY, Zhang Y, et al. Pyrometallurgical recycling of electric arc furnace dust. J Clean Prod 2017;149:1079–100, http://dx.doi.org/10.1016/j.jclepro.2017.02.128.

[6] Tsakiridis PE, Oustadakis P, Katsiapi A, Agatzini-Leonardou S. Hydrometallurgical process for zinc recovery from electric arc furnace dust (EAFD). Part II: downstream processing and zinc recovery by electrowinning. J Hazard Mater 2010;179:8–14, http://dx.doi.org/10.1016/j.jhazmat.2010.04.004.

[7] Nazari A, Shafyei A, Saidi A. Recycling of electric arc furnace dust into glass-ceramic. Mater Chem Phys 2018;205:436–41, http://dx.doi.org/10.1016/j.matchemphys.2017.11.045.

[8] Pelino M, Karamanov A, Pisciella P, Crisucci S, Zonetti D. Vitrification of electric arc furnace dusts. Waste Manag 2002;22:945–9, http://dx.doi.org/10.1016/S0956-053X(02)00080-6.

[9] Tsilika I, Komninou P. Structural characterization of Na2O-CaO-SiO2 glass ceramics reinforced with electric arc furnace dust. J Eur Ceram Soc 2007;27:2423–31, http://dx.doi.org/10.1016/j.jeurceramsoc.2006.09.011.

[10] Ledesma EF, Lozano-Lunar A, Ayuso J, Galvín AP, Fernández JM, Jiménez JR. The role of pH on leaching of heavy metals and chlorides from electric arc furnace dust in cement-based mortars. Constr Build Mater 2018;183:365–75, http://dx.doi.org/10.1016/j.conbuildmat.2018.06.175.

[11] Salihoglu G, Pinarli V, Salihoglu NK, Karaca G. Properties of steel foundry electric arc furnace dust solidified/stabilized with Portland cement. J Environ Manage 2007;85:190–7, http://dx.doi.org/10.1016/j.jenvman.2006.09.004.

[12] Hekal EE, Abo-El-Enein SA, El-Korashy SA, Megahed GM, El-Sayed TM. Utilization of electric arc furnace dust as an admixture to Portland cement pastes. J Therm Anal Calorim 2013;114:613–9, http://dx.doi.org/10.1007/s10973-013-2992-8.

[13] Salihoglu G, Pinarli V. Steel foundry electric arc furnace dust management: stabilization by using lime and Portland cement. J Hazard Mater 2008;153:1110–6, http://dx.doi.org/10.1016/j.jhazmat.2007.09.066.

[14] Laforest G, Duchesne J. Investigation of stabilization/solidification for treatment of electric arc furnace dust: dynamic leaching of monolithic specimens. Cem Concr Res 2007;37:1639–46, http://dx.doi.org/10.1016/j.cemconres.2007.08.025.

[15] Pereira CF, Rodríguez-Piero M, Vale J. Solidification/stabilization of electric arc furnace dust using coal fly ash: analysis of the stabilization process. J Hazard Mater 2001;82:183–95, http://dx.doi.org/10.1016/S0304-3894(00)00359-9.

[16] Fernández Pereira C, Luna Y, Querol X, Antenucci D, Vale J. Waste stabilization/solidification of an electric arc furnace dust using fly ash-based geopolymers. Fuel 2009;88:1185–93, http://dx.doi.org/10.1016/j.fuel.2008.01.021.

[17] Nikolić I, Đurović D, Blečić D, Zejak R, Karanović L, Mitsche S, et al. Geopolymerization of coal fly ash in the presence of electric arc furnace dust. Miner Eng 2013;49:24–32, http://dx.doi.org/10.1016/j.mineng.2013.04.007.

[18] Arnold MC, de Vargas AS, Bianchini L. Study of electric-arc furnace dust (EAFD) in fly ash and rice husk ash-based geopolymers. Adv Powder Technol 2017;28:2023–34, http://dx.doi.org/10.1016/j.apt.2017.05.007.

[19] Skaf M, Manso JM, Aragón Á, Fuente-Alonso JA, Ortega-López V. EAF slag in asphalt mixes: a brief review of its possible re-use. Resour Conserv Recycl 2017;120:176–85, http://dx.doi.org/10.1016/j.resconrec.2016.12.009.

[20] Autelitano F, Giuliani F. Electric arc furnace slags in cement-treated materials for road construction: mechanical and durability properties. Constr Build Mater 2016;113:280–9, http://dx.doi.org/10.1016/j.conbuildmat.2016.03.054.

[21] Santamaría A, Orbe A, Losañez MM, Skaf M, Ortega-Lopez V, González JJ. Self-compacting concrete incorporating electric arc-furnace steelmaking slag as aggregate. Mater Des 2017;115:179–93, http://dx.doi.org/10.1016/j.matdes.2016.11.048.
[22] Monosi S, Ruello ML, Sani D. Electric arc furnace slag as natural aggregate replacement in concrete production. Cem Concr Compos 2016;66:66–72, http://dx.doi.org/10.1016/j.cemconcomp.2015.10.004.
[23] Rondi L, Bregoli G, Sorlini S, Cominoli L, Collivignarelli C, Plizzari G. Concrete with EAF steel slag as aggregate: a comprehensive technical and environmental characterisation. Compos Part B Eng 2016;90:195–202, http://dx.doi.org/10.1016/j.compositesb.2015.12.022.
[24] Kim HS, Kim KS, Jung SS, Hwang JI, Choi JS, Sohn I. Valorization of electric arc furnace primary steelmaking slags for cement applications. Waste Manag 2015;41:85–93, http://dx.doi.org/10.1016/j.wasman.2015.03.019.
[25] Li Y, Meng X, Chen K, Barati M. Crystallization Behaviors of Spinel During Cooling Process of Modified EAF Slag. Metall Mater Trans B Process Metall Mater Process Sci 2020;51:1027–38, http://dx.doi.org/10.1007/s11663-020-01802-2.
[26] Nikolić I, Karanović L, Častvan IJ, Radmilović V, Mentus S, Radmilović V. Improved compressive strength of alkali activated slag upon heating. Mater Lett 2014;133:251–4, http://dx.doi.org/10.1016/j.matlet.2014.07.021.
[27] Provis JL. Activating solution chemistry for geopolymers. Geopolymers Struct. Process. Prop. Ind. Appl 2009:50–71, http://dx.doi.org/10.1533/9781845696382.1.50.
[28] Zhang YJ, Zhao YL, Li HH, Xu DL. Structure characterization of hydration products generated by alkaline activation of granulated blast furnace slag. J Mater Sci 2008;43:7141–7, http://dx.doi.org/10.1007/s10853-008-3028-9.
[29] Burciaga-Díaz O, Escalante-García JI. Structure, mechanisms of reaction, and strength of an alkali-activated blast-furnace slag. J Am Ceram Soc 2013;96:3939–48, http://dx.doi.org/10.1111/jace.12620.
[30] Krizan D, Zivanovic B. Effects of dosage and modulus of water glass on early hydration of alkali-slag cements. Cem Concr Res 2002;32:1181–8, http://dx.doi.org/10.1016/S0008-8846(01)00717-7.
[31] Barrett EP, Joyner LG, Halenda PP. The determination of pore volume and area distributions in porous substances. J Am Chem Soc 1951;73:373–80, http://dx.doi.org/10.1021/ja01145a126.
[32] Council of the European Union 2003/33/EC. Council Decision establishing criteria and procedures for the acceptance of waste at landfills pursuant to Article 16 of and Annex II to Directive 1999/31/EC. Off J Eur Communities 2003;11:27–49.
[33] Huang X, Zhuang RL, Muhammad F, Yu L, Shiau YC, Li D. Solidification/stabilization of chromite ore processing residue using alkali-activated composite cementitious materials. Chemosphere 2017:300–8, http://dx.doi.org/10.1016/j.chemosphere.2016.10.067.
[34] Malviya R, Chaudhary R. Factors affecting hazardous waste solidification/stabilization: a review. J Hazard Mater 2006;137:267–76, http://dx.doi.org/10.1016/j.jhazmat.2006.01.065.
[35] Puertas F, Palacios M, Manzano H, Dolado JS, Rico A, Rodriguez J. C-A-S-H gels formed in alkali-activated slag cement pastes. Structure and effect on cement properties and durability. MATEC Web Conf 2014;11, http://dx.doi.org/10.1051/matecconf/20141101002.
[36] Ya-min G, Yong-hao F, Duo Y, Yong-fan G, Chen-hui Z. Properties and microstructure of alkali-activated slag cement cured at below- and about-normal temperature. Constr Build Mater 2015;79:1–8, http://dx.doi.org/10.1016/j.conbuildmat.2014.12.068.
[37] Liu Z, Qian G, Zhou J, Li C, Xu Y, Qin Z. Improvement of ground granulated blast furnace slag on stabilization/solidification of simulated mercury-doped wastes in chemically bonded phosphate ceramics. J Hazard Mater 2008;157:146–53, http://dx.doi.org/10.1016/j.jhazmat.2007.12.110.
[38] Walkley B, San Nicolas R, Sani MA, Rees GJ, Hanna JV, van Deventer JSJ, et al. Phase evolution of C-(N)-A-S-H/N-A-S-H gel blends investigated via alkali-activation of synthetic calcium aluminosilicate precursors. Cem Concr Res 2016;89:120–35, http://dx.doi.org/10.1016/j.cemconres.2016.08.010.
[39] Morrow BA, McFarlan AJ. Surface vibrational modes of silanol groups on silica. J Phys Chem 1992;96:1395–400, http://dx.doi.org/10.1021/j100182a068.
[40] Raja K, Ramesh PS, Geetha D. Structural, FTIR and photoluminescence studies of Fe doped ZnO nanopowder by co-precipitation method. Spectrochim Acta - Part A Mol Biomol Spectrosc 2014;131:183–8, http://dx.doi.org/10.1016/j.saa.2014.03.047.
[41] Wilson MJ. Clay mineralogy: spectroscopic and chemical determinative methods; 1994, http://dx.doi.org/10.1007/978-94-011-0727-3.
[42] Garcia-Lodeiro I, Palomo A, Fernández-Jiménez A, MacPhee DE. Compatibility studies between N-A-S-H and C-A-S-H gels. Study in the ternary diagram Na2O-CaO-Al2O3-SiO 2-H2O. Cem Concr Res 2011;41:923–31, http://dx.doi.org/10.1016/j.cemconres.2011.05.006.
[43] Qian G, Sun DD, Tay JH. Characterization of mercury- and zinc-doped alkali-activated slag matrix: part II. Zinc. Cem Concr Res 2003;33:1257–62, http://dx.doi.org/10.1016/S0008-8846(03)00046-2.
[44] Yip CK, Lukey GC, Van Deventer JSJ. The coexistence of geopolymeric gel and calcium silicate hydrate at the early stage of alkaline activation. Cem Concr Res 2005;35:1688–97, http://dx.doi.org/10.1016/j.cemconres.2004.10.042.
[45] Garg N, White CE. Mechanism of zinc oxide retardation in alkali-activated materials: An: in situ X-ray pair distribution function investigation. J Mater Chem A Mater Energy Sustain 2017;5:11794–804, http://dx.doi.org/10.1039/c7ta00412e.
[46] Anseau MR, Leung JP, Sahai N, Swaddle TW. Interactions of silicate ions with zinc(II) and aluminum(III) in alkaline aqueous solution. Inorg Chem 2005;44:8023–32, http://dx.doi.org/10.1021/ic050594c.
[47] Ben Haha M, Le Saout G, Winnefeld F, Lothenbach B. Influence of activator type on hydration kinetics, hydrate assemblage and microstructural development of alkali activated blast-furnace slags. Cem Concr Res 2011;41:301–10, http://dx.doi.org/10.1016/j.cemconres.2010.11.016.
[48] Kumar R, Kumar S, Badjena S, Mehrotra SP. Hydration of mechanically activated granulated blast furnace slag. Metall Mater Trans B Process Metall Mater Process Sci 2005;36:873–83, http://dx.doi.org/10.1007/s11663-005-0089-x.
[49] Bernal SA, Provis JL, Walkley B, San Nicolas R, Gehman JD, Brice DG, et al. Gel nanostructure in alkali-activated binders based on slag and fly ash, and effects of accelerated carbonation. Cem Concr Res 2013;53:127–44, http://dx.doi.org/10.1016/j.cemconres.2013.06.007.
[50] Kim MS, Jun Y, Lee C, Oh JE. Use of CaO as an activator for producing a price-competitive non-cement structural binder using ground granulated blast furnace slag. Cem Concr Res 2013;54:208–14, http://dx.doi.org/10.1016/j.cemconres.2013.09.011.